Fizika Nizkih Temperatur, 2002, v. 28, No. 7, p. 677–690

Recent progress in magneto-optics and research on its application

(Review Article)

Norimichi Kojima

Graduate School of Arts and Sciences, The University of Komaba 3-8-1, Meguro-ku, Tokyo 153-8902, Japan
E-mail: cnori@mail.ecc.u-tokyo.ac.jp

Kuniro Tsushima

Kyushu Institute of Information Sciences, saifu 6-3-1, Dazaifu, Fukuoka 818-0117, Japan

Received April 10, 2002

We have investigated various kinds of magneto-optical properties for rare earth orthochromites. In $RCrO_3$(R = Tb, Dy and Ho), from the analysis of Cr^{3+} exciton absorption, it was elucidated that these compounds exhibit an anomalous spin-reorientation under the magnetic field along the *b* axis, where the weak ferromagnetic moment of the Cr^{3+} spins rotates in the *ac* plane perpendicular to the *b* axis. In these compounds, when the R^{3+} spin configuration is disordered, an anomalous satellite band appears in the lower energy side of the Cr^{3+} exciton absorption, which is associated with the breakdown of $\mathbf{k} = 0$ selection rule caused by the disorder of R^{3+} spin configuration. In $YbCrO_3$, various kinds of cooperative excitations such as Cr^{3+} exciton coupled with Yb^{3+} magnon and Cr^{3+}–Yb^{3+} exciton molecule appear in the visible region, which are induced by the antisymmetric exchange interaction between the Cr^{3+} and Yb^{3+} spins. The propagation of these cooperative excitations strongly depends on the spin structure and the external magnetic field. In $ErCrO_3$, a photo-induced spin-reorientation takes place within 50 μs after the photo-irradiation corresponding to the ${}^4A_{2g} \rightarrow {}^2E_g$ transition of Cr^{3+}, and it returns to the initial spin configuration in about 400 ms. This phenomenon was detected by the time-resolved Er^{3+} absorption spectra corresponding to the ${}^4I_{15/2} \rightarrow {}^4I_{9/2}$ transition. Finally, we briefly review the recent frontier research on application mainly developed in Japan.

PACS: 78.20.Ls

1. Introduction

It is our very great honor and a great pleasure to be able to submit our special review paper to celebrate and dedicate to Prof. V.V. Eremenko for his 70th birth. One of the authors (K.T.) has known him since 1960's and soon later both of us had a mutual opportunity to meet and discuss, for instance, at the time of the first and the second international symposium on magneto-optics, each as an organizer in Kyoto, 1987 [1], and in Kharkov, 1991 [2], respectively. We had also a frequent communication through long years, sometimes including his visit to Japan with his son. Every our communication with each other is an unforgettable remembrance.

More than 150 years ago, M. Faraday discovered that, when linearly polarized light propagates through a flint glass under an applied magnetic field, its plane of polarization is rotated. Since Faraday's original discovery, magneto-optics has become a highly fascinating field of research, which is of a great importance from the viewpoint of basic science and application. Especially, the magneto-optics and spectroscopy of magnetically ordered materials have actively been developing since 1960s. Recently, Eremenko et al. [3], Zvezdin and Kotov [4], and Sugano and Kojima [5] have edited the books in which recent fascinating topics of magneto-optical properties are described.

In magnetically ordered materials, various kinds of magneto-optical properties appear as the syner-

gistic effect between optical properties and magnetic properties. The magnetic interaction between elementary excitations such as excitons and magnons enables them to combine with one another, forming new and more complex excitations such as exciton–magnon transitions, which are observed in the visible region. Moreover, both the magnetic interaction and spin structure have effects on the propagation, the energy position and the shape of elementary excitations. Therefore, the analysis of magneto-optical properties is one of the most powerful tools to investigate the spin configurations and magnetic phase transitions.

In this paper, we describe various kinds of magneto-optical properties of rare earth orthochromites and review the recent frontier research on application. In Sec. 2, we report an anomalous field-induced spin-reorientation in $RCrO_3$(R = Tb, Dy and Ho) by the analysis of Cr^{3+} exciton absorption. Moreover, we describe the breakdown of $k = 0$ selection rule for the Cr^{3+} exciton absorption in $RCrO_3$(R = Dy and Ho) induced by the disorder of the R^{3+} spin configuration. In Sec. 3, we describe various types of cooperative excitations in $YbCrO_3$ induced by the Cr^{3+}–Yb^{3+} exchange interaction. Moreover, we describe that the Cr^{3+}–Yb^{3+} antisymmetric exchange interaction depends on the dynamics of their cooperative excitations. In Sec. 4, after the survey of the recent progress of photo-induced magnetism, we describe our pioneering work of the photo-induced spin-reorientation in $ErCrO_3$. In Sec. 5, we survey the recent frontier research on application especially developed in Japan.

2. Optical investigation of various magnetic phase transition

It is well known that electronic excitations of several electronvolts in magnetic insulators can be regarded as transitions within an incomplete *d* or *f* shell of a single magnetic ion. Such a localized excitation cannot, however, be an eigenstate of the crystal, and excitation migrates on magnetic ions as an excitation wave called as Frenkel exciton. This property is reflected in the energy dispersion and the Davydov splitting. In magnetically ordered state, the analysis of Frenkel exciton is one of the most powerful methods to elucidate the spin configuration and magnetic phase transitions, because the magnetic symmetry change associated with phase transition is directly reflected in the selection rule of the polarized exciton lines.

In this Section, we elucidate an anomalous-type of spin-reorientation in rare earth orthochromites,

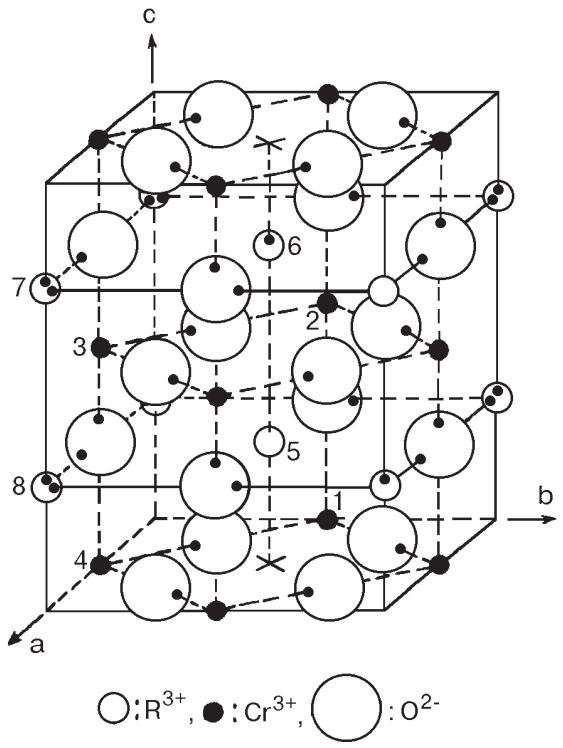

Fig. 1. Unit cell of $RCrO_3$. The Cr^{3+} and R^{3+} positions are indicated with numbers *1–4* and *5–8*, respectively.

$RCrO_3$(R = Ho, Dy, and Tb), by the analysis of Cr^{3+} exciton lines.

$RCrO_3$ has an orthorhombically distorted perovskite structure belonging to the space group P_{bnm} (D_{2h}^{16}) [6]. The unit cell contains four molecules as shown in Fig. 1. The Cr^{3+} spins order spontaneously at Néel temperature (T_{N1}) and these compounds generally exhibit a weak ferromagnetic moment. At the second Néel temperature (T_{N2}), the R^{3+} spins begin to reorder antiferromagnetically. The allowed spin configurations for the Cr^{3+} and R^{3+} sites at $T_{N1} < T < T_{N2}$ are shown in Fig. 2. The allowed spin configurations are denoted as $\Gamma_1(A_xG_yC_z;C_z^{R})$, $\Gamma_2(F_xC_yG_z;F_x^{R}C_y^{R})$, and $\Gamma_4(G_xA_yF_z;F_z^{R})$ in Bertaut notation [7].

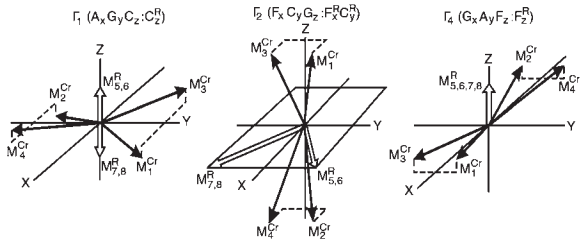

Fig. 2. Spin configuration of $RCrO_3$ at $T_{N2} < T < T_{N1}$.

2.1. Field induced spin-reorientation in $HoCrO_3$

It is well known that $RCrO_3$ and $RFeO_3$ exhibit various types of field induced spin reorientation where the weak ferromagnetic moment becomes parallel to the direction of the applied magnetic field. In the cases of $H_0 \parallel a$ and c, the spin reorientations of $(\Gamma_1, \Gamma_4) \to \Gamma_2$ and $(\Gamma_1, \Gamma_2) \to \Gamma_4$ have been reported for various $RCrO_3$ and $FeCrO_3$. In the case of $H_0 \parallel b$, on the other hand, any spin reorientation is not expected, because any spin configuration with a weak ferromagnetic moment of the Cr^{3+} spins along the b axis can not be allowed in the absence of an external magnetic field. However, Courths et al. and we have observed an abrupt spectral change in $HoCrO_3$ at 1.8 K with the magnetic field $H_0 \approx 20$ kOe along the b axis, and they have suggested that this spectral change at 20 kOe is interpreted as a spin reorientation where the weak ferromagnetic moment of the Cr^{3+} spins rotates in the ac plane perpendicular to the b axis [8,9].

In $HoCrO_3$, the Cr^{3+} spins are antiferromagnetically ordered below $T_{N1} = 140$ K with a weak ferromagnetic moment as $\Gamma_2(F_xC_yG_z;F_x{}^RC_y{}^R)$ [10]. Any additional transition has not been observed down to 1.5 K. As shown in Fig. 2, in the case of Γ_2 spin configuration, the Cr^{3+} sublattice magnetic moments and the Cr^{3+} net magnetic moment lie along the c axis and the a axis, respectively. The anisotropy axes of the Ho^{3+} ions lie in the ab plane at about ±65° from the a axis [10], and the g values along the a, b and c axes are 7.3, 15.7, and 0, respectively [8], where the magnitude of the effective spin of Ho^{3+} is $1/2$. Therefore, the Ho^{3+} spins are strictly confined in the ab plane.

Figure 3 shows the behavior of the energies of the absorption spectra around 13700 cm^{-1} for $HoCrO_3$ in the magnetic field $H_0 \parallel b$ at 1.5 K. In this energy region, four sharp lines (R_1, R_2, R_3, and R_4) of magnetic dipole character are observed. The four magnetic dipole lines are assigned to the Davydov-split components of the Cr^{3+} exciton corresponding to the transition from the lowest substate of ${}^4A_{2g}$ to the lowest substate of ${}^2E_g$. As shown in Fig. 3, when the magnetic field is applied along the b axis, the $R_{1\text{-}4}$ lines split into two pairs of R_1, R_2 and R_3, R_4 in the range of 10 to 20 kOe, and at about 20 kOe, an abrupt spectral change occurs. As the magnetic field increases from 19.5 to 20.5 kOe, the R lines for the lower magnetic field phase vanish, while those for the higher magnetic field phase grow up. The discontinuous variation of the energies of R lines and the existence of both phases in a small field region (~1 kOe) around the

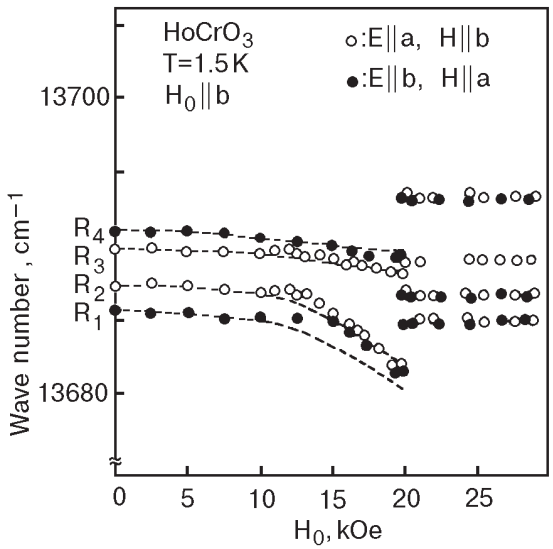

Fig. 3. Magnetic field dependence of the lowest energy region of the ${}^4A_{2g} \to {}^2E_g$ transition of Cr^{3+} in $HoCrO_3$. E and H denote the electric and magnetic vectors of the incident light, respectively. Solid and open circles: experimental points. Broken lines: calculated energy shifts of the R lines corresponding to the transition from the lowest substate of ${}^4A_{2g}$ to the lowest substate of ${}^2E_g$ of Cr^{3+} by setting $\tilde{D}_x = \tilde{D}'_x = 1.2$ cm^{-1} and $\tilde{D}_y = \tilde{D}'_y = 1.2$ cm^{-1} .

critical field H_c (~20 kOe) indicate that this phase transition is of first order. The energies, polarizations and intensities of the R lines show notable changes at this phase transition, which suggests the occurrence of the spin reorientation of Cr^{3+}. Above 20 kOe, the energies of R lines remain unchanged, which indicates that the antiferromagnetic axis in the higher magnetic field phase is perpendicular to the b axis. Therefore, it is obvious that the spin configurations of the Cr^{3+} spins below and above H_c are Γ_2 ($F_xC_yG_z$) and $\Gamma_4(G_x A_y F_z)$, respectively.

The remarkable splitting of the R lines in the external magnetic field region between 10 kOe and 20 kOe are explained as follows. The molecular field H_B ($\parallel c$) on the $S_{i=1}^{Cr}$ spin induced by the Cr^{3+}– Ho^{3+} exchange interaction is expressed as,

$$g_c^{Cr}\beta H_B = 4\left(\tilde{D}_y\left\langle S_{5x}^{Ho}\right\rangle + \tilde{D}'_y\left\langle S_{7x}^{Ho}\right\rangle\right) - 4\left(\tilde{D}_x\left\langle S_{5y}^{Ho}\right\rangle - \tilde{D}'_x\left\langle S_{7y}^{Ho}\right\rangle\right) \quad (1)$$

and that on the $S_{i=3}^{Cr}$ spin is expressed as

$$g_c^{Cr}\beta H_B = 4\left(\tilde{D}_y\left\langle S_{5x}^{Ho}\right\rangle + \tilde{D}'_y\left\langle S_{7x}^{Ho}\right\rangle\right) + 4\left(\tilde{D}_x\left\langle S_{5y}^{Ho}\right\rangle - \tilde{D}'_x\left\langle S_{7y}^{Ho}\right\rangle\right) \quad (2)$$

where, $\tilde{D}_x$, $\tilde{D}'_x$, $\tilde{D}_y$, and $\tilde{D}'_y$ denote the antisymmetric exhange interaction constants between Cr^{3+} and Ho^{3+}. In the absence of external magnetic field, the molecuar fields H_B on the four inequivalent are Cr^{3+} spins due to the Cr^{3+} – Ho^{3+} interaction are equal because of $\left\langle S_{jx}^{\mathrm{Ho}}(j=5,6)\right\rangle = \left\langle S_{jx}^{\mathrm{Ho}}(j=7,8)\right\rangle$ and $\left\langle S_{jy}^{\mathrm{Ho}}(j=5,6)\right\rangle = -\left\langle S_{jy}^{\mathrm{Ho}}(j=7,8)\right\rangle$. However, when the magnetic field is applied along the *b* axis, $\left\langle S_{j}^{\mathrm{Ho}}(j=7,8)\right\rangle$ change and then the molecular fields on the $S_{i=1,2}^{\mathrm{Cr}}$ spins due to the Cr^{3+} – Ho^{3+} interaction become different from those on the $S_{i=3,4}^{\mathrm{Cr}}$ spins, which causes the remarkable splitting of the *R* lines in the magnetic field region between 10 and 20 kOe. The broken lines in Fig. 3 show the calculated energy shifts of the *R* lines with $H_0 \parallel b$, by setting $\tilde{D}_x$=$\tilde{D}'_x$= 1.2 cm^{-1} and $\tilde{D}_y$=$\tilde{D}'_y$= 1.2 cm^{-1}. In this calculation, we assumed that the molecular field for the ^2E_g state is equal to that for the ground state. As shown in Fig. 3, the behavior of the *R* lines in the magnetic field region $H_0 < H_c$ is well reproduced in the calculation.

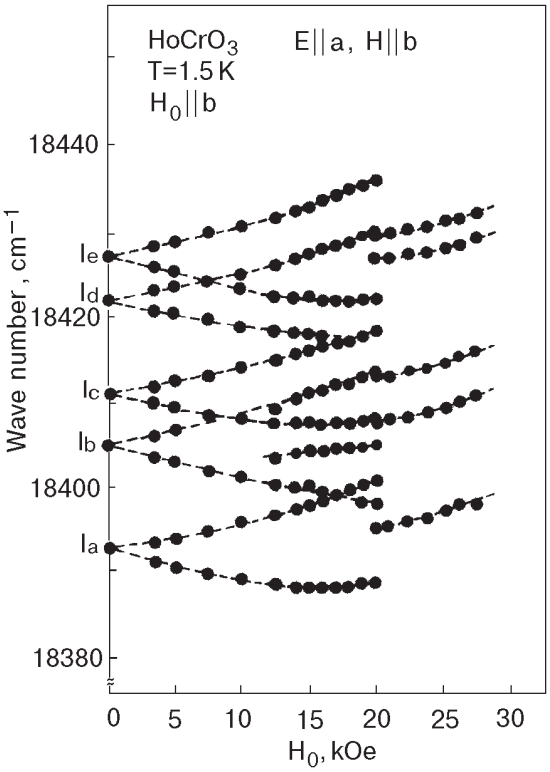

Fig. 4. Magnetic field dependence of the $^5I_8 \rightarrow {}^5S_2$ transition of Ho^{3+} in $HoCrO_3$.

In order to confirm the above mentioned result, we have investigated the behavior of the $^5I_8 \rightarrow {}^5S_2$ transition of Ho^{3+} in the magnetic field $H_0 \parallel b$ at T= 1.5 K, which is shown in Fig. 4. At T = 1.5 K, only the transitions from the lowest energy level *I* of the ground multiplet ($^5I_8$) to the five singlet states of $^5S_2$ labeled as I_a , I_b , I_c , I_d, and I_e in order of increasing energy can be observed. As shown in Fig. 4, when an external magnetic field is applied up to H_c, the I_a–I_e lines split and the splitting increases with increasing magnetic field. However, the splitting vanishes at H_c. If the spin configuration of Cr^{3+} is $\Gamma_2(F_xC_yG_z)$, the effective field on the Ho^{3+} site with $S_y^{\mathrm{Ho}} = S$ is different from that with $S_y^{\mathrm{Ho}} = -S$ when the e{xternal field is applied along the *b* axis, which causes the so-called sublattice splitting. Then, the splitting of I_a – I_e lines in the magnetic field region of $H_0 < H_c$ is interpreted as the sublattice splitting of the $^5I_8 \rightarrow {}^5S_2$ transition.

In the case of $H>H_c$, from the analysis of Cr^{3+} exciton lines, the spin configuration is considered to be Γ_4 ($G_xA_yF_z$), where the molecular field on the Ho^{3+} spin becomes parallel to the *c* axis and its value should be nearly zero because g_c^{Ho} is negligibly small. Therefore, in the higher magnetic field phase ($H_0 > H_c$), the Ho^{3+} spins are arrayed only by the external magnetic field ($H_0 \parallel b$), and the Zeeman energies upon the four Ho^{3+} sites are equal. Thus, the sublattice splitting of I_a – I_e lines corresponding to the $^5I_8 \rightarrow {}^5S_2$ transition of Ho^{3+} vanish above H_c (= 20 kOe). Thus, we can determine the spin configurations of $HoCrO_3$ in various magnetic fields of $H_0 \parallel b$, which is schematically shown in Fig. 5.

2.2. Field induced spin-reorientation in $TbCrO_3$

The Cr^{3+} spins in $TbCrO_3$ are antiferromagnetically ordered below T_{N1} = 167 K with a weak ferromagnetic moment as $\Gamma_2(F_xC_yG_z;F_x^{\mathrm{R}}C_y^{\mathrm{R}})$ [11]. The Tb^{3+} spins are antiferromagnetically ordered below T_{N2} = 3.1 K, and the spin configuration below T_{N2} is denoted as $\Gamma_{25}(F_xC_yG_z: F_x^{\mathrm{R}}C_y^{\mathrm{R}}; G_x^{\mathrm{R}}A_y^{\mathrm{R}})$ [11]. The easy axes of Tb^{3+} spins lie in the *ab* plane at about

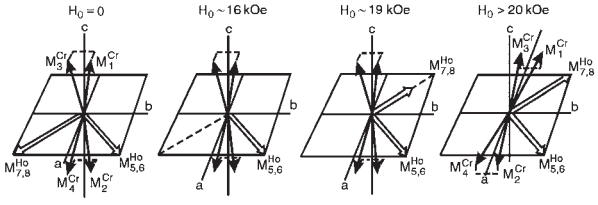

Fig. 5. Spin configurations of $HoCrO_3$ in various magnetic fields at 1.5 K. The magnetic field $H_0 \parallel b$.

± 45° from the *a* axis. The *g* values along the *a*, *b*, and *c* axes are 12.6, 12.6, and 0, respectively [12], where the magnitude of the effective spin of Tb^{3+} is 1/2. Therefore, the Tb^{3+} spins are strictly confined in the *ab* plane.

Figure 6 shows the behavior of the Davydov-split components of the Cr^{3+} exciton line corresponding to the ${}^4A_{2g} \rightarrow {}^2E_g$ transition in $TbCrO_3$. As shown in Fig. 6, when the magnetic field is applied along the *b* axis, the $R_{1\text{-}4}$ lines split into two pairs of R_1, R_2 and R_3, R_4 in the magnetic field region between 8 and 15 kOe. At about 15 kOe, the energies, polarizations, and intensities of the *R* lines show notable changes, which resembles closely the behavior of the *R* lines in $HoCrO_3$ at the spin-reorientation from Γ_2 to Γ_4. Therefore, it is obvious that the spin configurations of the Cr^{3+} spins in $TbCrO_3$ below and above H_c(= 15 kOe) are Γ_2 ($F_xC_yG_z$) and Γ_4 ($G_xA_yF_z$), respectively.

In the magnetic field region below H_c, with increasing external field, the energy gravity of the *R* lines drops around 8 kOe and then it remains unchanged. The drop in the energy of *R* lines at about 8 kOe is attributed to the spin flip of the $Tb_6{}^{3+}$ and $Tb_7{}^{3+}$ sites. Thus, we can determine the spin configurations of $TbCrO_3$ in various magnetic fields of $H_0 \parallel b$, which is schematically shown in Fig. 7.

2.3. Field induced spin-reorientation in $DyCrO_3$

The Cr^{3+} spins in $DyCrO_3$ are antiferromagnetically ordered below T_{N1} = 146 K with a weak ferromagnetic moment as $\Gamma_2(F_xC_yG_z;\ F_x{}^RC_y{}^R)$

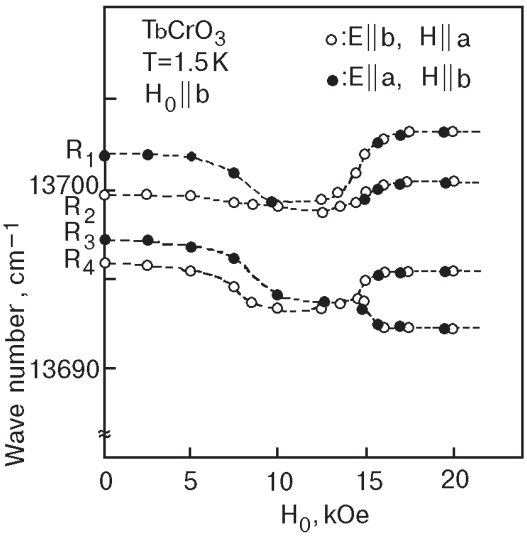

Fig. 6. Magnetic field dependence of the *R* lines of $TbCrO_3$. Broken lines are the guide for eye.

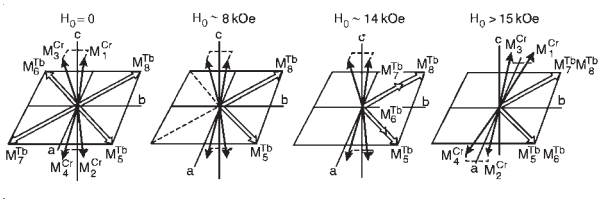

Fig. 7. Spin configurations of $TbCrO_3$ in various magnetic fields at 1.5 K. The magnetic field $H_0 \parallel b$.

[13]. The Dy^{3+} spins are antiferromagnetically ordered below T_{N2} = 2.0 K, and the spin configuration below T_{N2} is denoted as $\Gamma_{25}(F_xC_yG_z: F_x{}^RC_y{}^R; G_x{}^RA_y{}^R)$ [13]. The easy axes of Dy^{3+} spins lie in the *ab* plane at about ±60° from the *a* axis. The *g* values along the *a*, *b*, and *c* axes are 6.0, 17.0, and 0, respectively [14], where the magnitude of the effective spin of Dy^{3+} is 1/2. Therefore, the Dy^{3+} spins are strictly confined in the *ab* plane.

Figure 8 shows the behavior of the Davydov-split components of the Cr^{3+} exciton line corresponding to the ${}^4A_{2g} \rightarrow {}^2E_g$ transition in $DyCrO_3$. When the magnetic field is applied along the *b* axis, the energies, polarizations and intensities of the *R* lines dramatically change at about 2 kOe. Above 3 kOe,

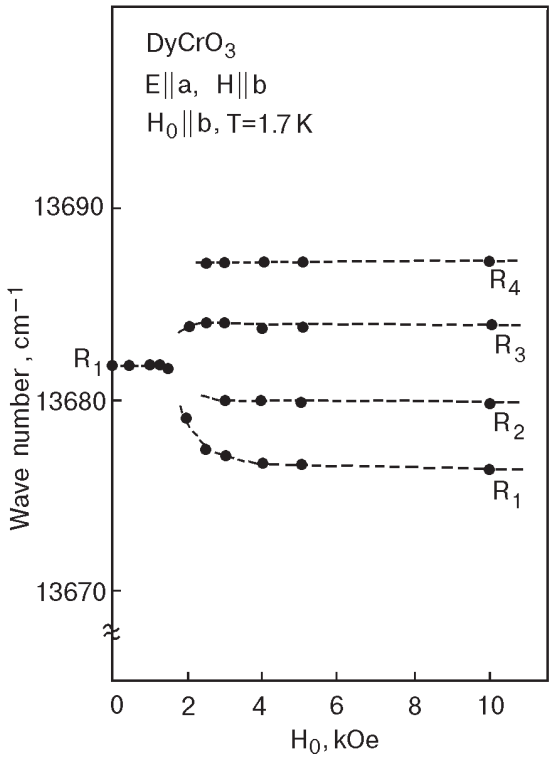

Fig. 8. Magnetic field dependence of the *R* lines of $DyCrO_3$. Broken lines are the guide for eye.

those of the R lines remain unchanged. From the analogy of the behavior of R lines in $HoCrO_3$ and $TbCrO_3$, $DyCrO_3$ exhibits the field induced spin reorientation from $\Gamma_2(F_xC_yG_z)$ to $\Gamma_4(G_xA_yF_z)$ at $H_0(\| b) = 2$ kOe.

2.4. Breakdown of the **k** *= 0 selection rule of Frenkel exciton*

In the optical absorption corresponding to the pure Frenkel exciton, only the zone-center exciton is observable, because the magnitude of the propagation vector of visible light is of the order of 10^{-3} reciprocal lattice vectors, which is usually called **k** = 0 selection rule. However, in the cases of mixed crystals or amorphous materials, it is predicted that the deviation from a periodic structure causes the breakdown of the **k** = 0 selection rule for the exciton transition. Impurities, alloy and interface roughness occurring on the length scale of unit cell are the best known examples which provide an appropriate momentum of elastic scattering. Thus, the deviation from the virtual crystal causes the $\mathbf{k} \neq 0$ (nonvertical) transition through the medium of the momentum of elastic scattering. In fact, the disorder-induced optical transitions for the mixed crystals such as $AgCl_{1-x}Br_x$ [15], $GaAs_{1-x}P_x$ [16] and $Al_xGa_{1-x}As$ [17] have characteristics which can be associated with the breakdown of the **k** selection rule for a periodic structure.

However, the breakdown of **k** = 0 selection rule induced by the disorder of spin-configuration has not yet been elucidated. In this Section, we report the breakdown of **k** = 0 selection rule for the Cr^{3+} exciton absorption in $RCrO_3$(R = Ho and Dy) induced by the disorder of the R^{3+} spin configuration.

Figure 9 shows the field dependence of the optical absorption spectra corresponding to the lowest energy region of the ${}^4A_{2g} \rightarrow {}^2E_g$ transition of Cr^{3+} in $HoCrO_3$ [18]. The R_2 and R_3 lines are the Davydov-split components of the pure Cr^{3+} exciton. When an external magnetic field is applied along the b axis at 1.5 K, an anomalous satellite band (R') appears in the lower energy side of R lines at about 7.5 kOe and its intensity passes through a maximum at 16 kOe and then disappears at H_c= 20 kOe. As mentioned already, when the external magnetic field is increased along the b axis of $HoCrO_3$, the sublattice magnetic moments, $\mathbf{M}_7^{Ho}$ and $\mathbf{M}_8^{Ho}$ due to the S_7^{Ho} and S_8^{Ho} spins decrease and vanish at about 16 kOe, and above 16 kOe they grow gradually toward the direction of the applied magnetic field. On the other hand, $\mathbf{M}_5^{Ho}$ and $\mathbf{M}_6^{Ho}$ are saturated in the whole field range. From the behavior of the R' band and the spin configuration of $HoCrO_3$ in the magnetic field along the b axis, it is obvious that the transition responsible for the R' satellite band in $HoCrO_3$ is allowed when the spin configuration of the Ho^{3+} sites is disordered.

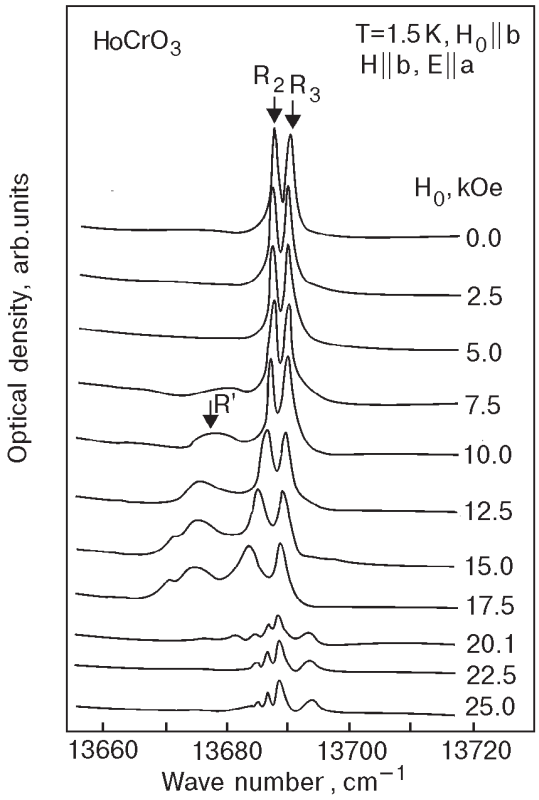

Fig. 9. Behavior of the R lines and the R' band of $HoCrO_3$ under magnetic fields along the b axis.

Figure 10 shows the field dependence of the optical absorption spectra corresponding to the lowest energy region of the ${}^4A_{2g} \rightarrow {}^2E_g$ transition of Cr^{3+} in $DyCrO_3$. The R_1 line is the Davydov-split component of the pure Cr^{3+} exciton. When an external magnetic field is applied along the b axis at 1.7 K, the intensity of the R' satellite band increases abruptly at 1.5 kOe, and then decreases rapidly. As shown in the inset of Fig. 10, when the external magnetic field is applied along the b axis at 1.8 K, the metamagnetic transition takes place at 1.5 kOe, where the magnetic moments due to the S_6^{Dy} and S_7^{Dy} spins are going to reverse their directions from being antiparallel to parallel to the external magnetic field. Therefore, it is obvious that the transition responsible for the R' satellite band in $DyCrO_3$ is allowed when the spin configuration of the Dy^{3+} sites is disordered.

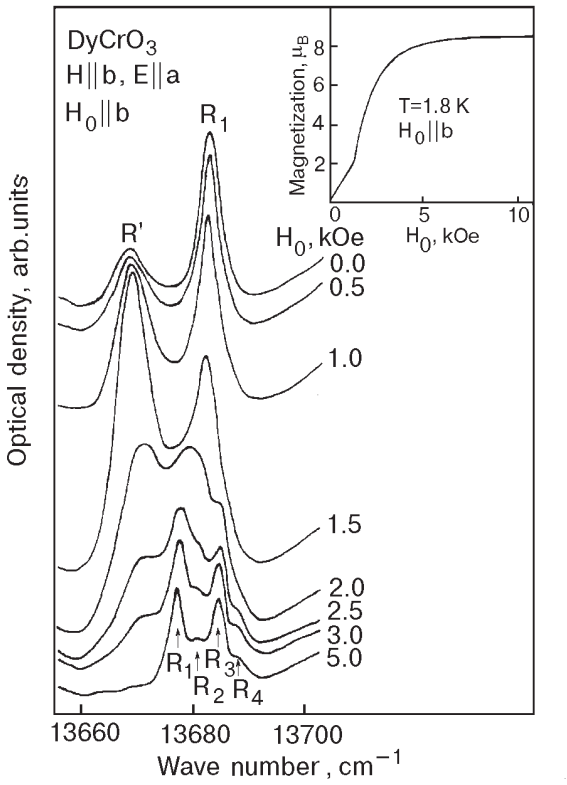

Fig. 10. Behavior of the R lines and the R' band of $DyCrO_3$ under magnetic fields along the b axis at 1.8 K. Inset shows the magnetization curve.

The characteristic properties of the R' satellite band in $RCrO_3$(R = Ho and Dy) are summarized as follows. 1. The energy of the R' band is lower by about 16 cm^{-1} than the average energy of the pure Cr^{3+} exciton lines. 2. The dipole nature of the R' band is poorly characterized, while that of the pure Cr^{3+} exciton lines is explicitly magnetic. 3. The field induced energy shift of the R' band disagrees with the sum of the energy shift of Cr^{3+} exciton and the R^{3+} spin flip, which implies that the R' band does not correspond to the Cr^{3+} exciton coupled with R^{3+} spin flip. 4. The transition responsible for the R' band is allowed when the R^{3+} spin configuration is disordered by temperature or external magnetic field. 5. As the magnetic moment of the R^{3+} spins approaching saturation, the R' band disappears.

Now, we discuss the transition mechanism responsible for the R' band in $RCrO_3$(R = Ho and Dy). The Cr^{3+} exciton dispersion due to the spin allowed transfer is expressed as,

$$E(k) = E_0 + 2V_{11}{}^a \cos(ak_x) + 2V_{11}{}^b \cos(bk_y) \pm \\ \pm 8V_{13}\cos(ak_x/2)\cos(bk_y/2)\cos(ck_z/2), \quad (3)$$

where E_0 is the relevant excitation energy for the single Cr^{3+} ion, $V_{11}{}^a$ and $V_{11}{}^b$ represent the intra-sublattice transfers along the a and b axes, respectively, and V_{13} the spin allowed inter-sublattice one. From the analysis of the absorption spectra corresponding to the Cr^{3+} exciton coupled with R^{3+} magnon in $RCrO_3$(R = Tm and Yb), the Cr^{3+} exciton due to the ${}^4A_{2g} \rightarrow {}^2E_g$ transition has a large negative dispersion whose values for $TmCrO_3$ and $YbCrO_3$ are estimated at −14 cm^{-1} and −16 cm^{-1} [19,20], respectively. Therefore, it is plausible that the sign and the magnitude of the Cr^{3+} exciton dispersion in $HoCrO_3$ and $DyCrO_3$ are almost the same as those of the Cr^{3+} exciton dispersion in $TmCrO_3$ and $YbCrO_3$. Figure 11,*b* shows the energy dispersion of the Cr^{3+} exciton due to the ${}^4A_{2g} \rightarrow {}^2E_g$ transition in $YbCrO_3$, where $V_{11}{}^a = 3.0$ cm^{-1} and $V_{11}{}^b = 1.0$ cm^{-1}. As shown in Fig. 11, the energy position of the R' band in $RCrO_3$(R = Ho and Dy) agrees very closely with that of the Cr^{3+} exciton at the Brillouin-zone boundary, which implies that the R' band is assigned to the excitation of the pure Cr^{3+} exciton at the zone boundary, which is caused by the disorder of the R^{3+} spin configuration. However, in general, the optical excitation of the pure Cr^{3+} exciton at the zone boundary cannot be observed without the breakdown of the $\mathbf{k} = 0$ selection rule.

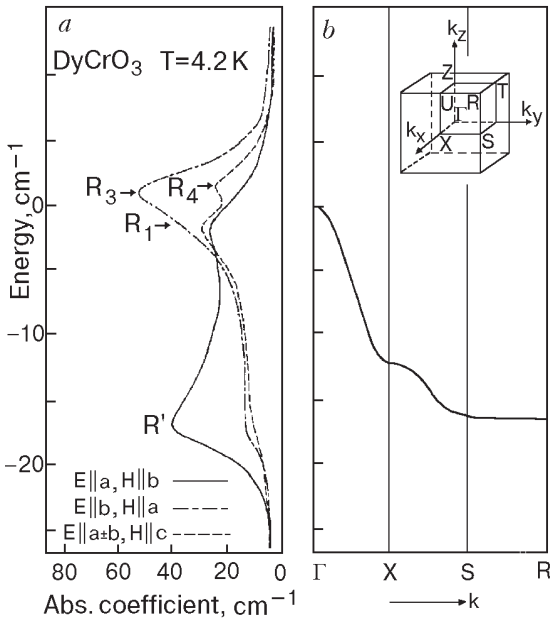

Fig. 11. (*a*) R lines and R' band of $DyCrO_3$, (*b*) Cr^{3+} exciton dispersion in $YbCrO_3$. The origin of the energy is fixed at the average energy of the free Cr^{3+} exciton lines.

Thus, we arrives at the following conclusion. The magneto-elastic effect due to the R^{3+} (R = Ho and Dy) ion is extraordinarily large because of the strong spin-orbit interaction. When the R^{3+} spins are fluctuated by temperature or external magnetic field, the disorder of the R^{3+} spin configuration deforms the periodic lattice potential. Through the medium of the strong magneto-elastic effect, the disorder of the R^{3+} spin configuration causes the breakdown of the $\mathbf{k} = 0$ selection rule of the Cr^{3+} exciton absorption and it is reflected in the appearance of the R' satellite band in the lower energy side of the free Cr^{3+} exciton.

3. Various cooperative excitations

In magnetically ordered materials, various types of elementary excitations such as excitons and magnons exist. The magnetic interaction between these elementary excitations enables them to combine with one another, forming cooperative excitations such as exciton-magnon transition [21], which are observed in the visible region. In this Section, we describe two kinds of cooperative excitations induced by $3d$–$4f$ exchange interaction in $YbCrO_3$. Figure 12 shows the optical absorption spectra of $YbCrO_3$ in the energy region from visible to near-infrared at 1.5 K. The absorption spectra of $YbCrO_3$ in the energy region between 10000 cm^{-1} and 25000 cm^{-1} are assigned as shown in Fig. 12. In this energy region, besides the elementary excitations due to d–d and f–f transition and the cooperative excitations induced by the $3d$–$3d$ and $4f$–$4f$ exchange interactions, various kinds of cooperative excitations induced by the $3d$–$4f$ exchange interaction are observed. The Yb^{3+} exciton–Cr^{3+} magnon excitation is observed in the ${}^2F_{7/2} \rightarrow {}^2F_{5/2}$ transition of Yb^{3+} [22], and the Cr^{3+} exciton – Yb^{3+} magnon excitation is observed in the ${}^4A_{2g} \rightarrow {}^2E_g$ transition of Cr^{3+} [20]. Moreover, the Cr^{3+} exciton –Yb^{3+} exciton excitation is observed in the higher energy side of the ${}^4A_{2g} \rightarrow {}^4T_{1g}$ transition of Cr^{3+} [23].

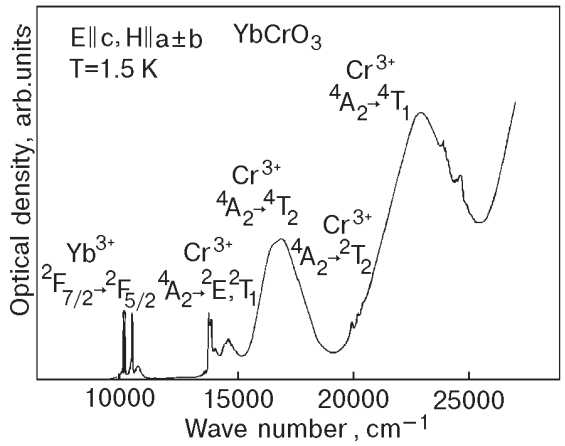

Fig. 12. Optical absorption spectra of $YbCrO_3$ in the energy region from visible to near-infrared.

Here, we briefly summarize the magnetic properties of $YbCrO_3$. In $YbCrO_3$, there are three types of magnetic interactions, Cr^{3+}–Cr^{3+}, Cr^{3+}–Yb^{3+}, and Yb^{3+}–Yb^{3+}, each of which generally consists of the isotropic, and the anisotropic symmetric and antisymmetric exchange interactions. Among various $RCrO_3$, $YbCrO_3$ is an interesting one with a strong anisotropic exchange interaction between the Cr^{3+} and Yb^{3+} ions [24]. In the case of Yb^{3+} ion having only one $4f$ hole, the $4f$ orbital is widely spread, which is responsible for the strong $3d$–$4f$ exchange interaction in $YbCrO_3$. The strong anisotropic exchange interaction between the Cr^{3+} and Yb^{3+} spins in $YbCrO_3$ is able to induce various kinds of cooperative excitations. The Cr^{3+} spins in $YbCrO_3$ are antiferromagnetically ordered below T_{N1} = 118 K with a weak ferromagnetic moment as $\Gamma_2(F_xC_yG_z;F_x{}^RC_y{}^R)$ [25]. The spontaneous magnetic moment of $YbCrO_3$ crosses to zero at 16.5 K, which reveals that the induced magnetic moment of the Yb^{3+} spins couples antiparallel to the weak ferromagnetic moment of the Cr^{3+} spins [25].

3.1. Cooperative excitation between Cr^{3+} exciton and Yb^{3+} magnon

Figure 13 shows the absorption spectra corresponding to the lowest energy region of the ${}^4A_{2g} \rightarrow {}^2E_g$ transition of Cr^{3+} in $YbCrO_3$. The R_1 and R_3 lines with magnetic dipole character are assigned to the Davydov-split components of the pure Cr^{3+} exciton. In the neighborhood of the Cr^{3+} exciton lines, an electric dipole band (R' band) appears, which has an anomalous band shape with a sharp cut-off at the lower energy side and fine structure. The R' band corresponds to the cooperative excitation of Cr^{3+} exciton and Yb^{3+} magnon. The band width and the cut-off profile at the lower energy side of the R' band could be reproduced quantitatively by taking account of the negative exciton dispersion of -16 cm^{-1} [20].

As shown in Fig. 13, when the external magnetic field is applied along the a axis of $YbCrO_3$ at 2.0 K, a sharp and strong peak (arrow in Fig. 13) typical of bound state appears on the lowest energy side of the R' band. At about 25 kOe, the bound state grows most strongly. Above 30 kOe, the bound state splits into several peaks and their intensity decreases significantly. At about 68 kOe, a

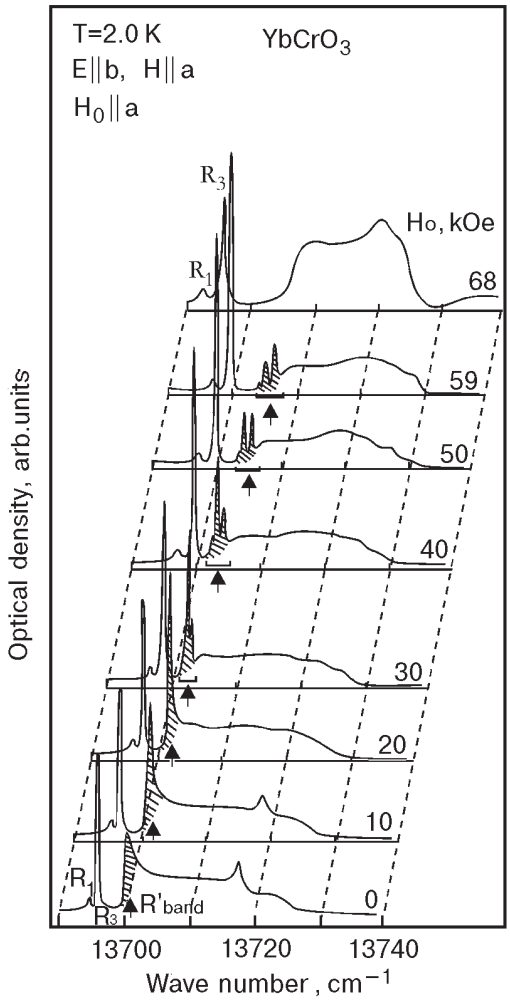

Fig. 13. Behavior of the R lines and the R' band of $YbCrO_3$ under magnetic fields along the a axis at 2.0 K. Arrow shows the bound state of the R' band.

dramatic spectral change occurs. The discontinuous spectral change between 59 kOe and 68 kOe is due to the metamagnetic phase transition (H_c) where the weak ferromagnetic moment of the Cr^{3+} spins reverses its direction from being antiparallel to parallel to the net magnetic moment of the Yb^{3+} spins. At this metamagnetic transition [26], the profile of the R' band changes drastically and its bound state disappears completely.

From the appearance of the bound state on the lowest energy side of the R' band, we arrive at the following concept. The Cr^{3+} exciton coupled with Yb^{3+} magnon at the Brillouin-zone edge is localized under the external magnetic field ($H_0 \parallel a$), while the Cr^{3+} exciton coupled with Yb^{3+} magnon at any point of the Brillouin-zone except the zone edge is delocalized. At 25 kOe, the Cr^{3+} exciton coupled with Yb^{3+} magnon at the Brillouin-zone edge is most strongly localized, which is reflected in the field dependent energy shift of the R' band. Since the R' band is assigned to the cooperative excitation between Cr^{3+} exciton and Yb^{3+} magnon, the magnetic field dependent shift of the energy separation ($\Delta E\ (H_0)$) between the R' band and the Cr^{3+} exciton lines should be expressed as,

$$\Delta E(H_0) = \Delta E_{R'}(H_0) - \Delta E_R(H_0) = \Delta E_{\mathrm{Yb}}(H_0), \quad (4)$$

with

$$\Delta E_{R'}(H_0) = E_{R'}(H_0) - E_{R'}(H_0 = 0),$$

$$\Delta E_R(H_0) = E_R(H_0) - E_R(H_0 = 0),$$

$$\Delta E_{\mathrm{Yb}}(H_0) = E_{\mathrm{Yb}}(H_0) - E_{\mathrm{Yb}}(H_0 = 0), \quad (5)$$

where, $E_{R'}(H_0)$ and $E_R(H_0)$ denote the energy position of the lowest energy side of the R' band and that of the average energy of the R lines under the external magnetic field ($H_0 \parallel a$), respectively, and $E_{\mathrm{Yb}}(H_0)$ denotes the energy of the Yb^{3+} magnon under the external magnetic field ($H_0 \parallel a$), which is estimated from the analysis of the Yb^{3+} exciton – Yb^{3+} magnon excitation appearing in the ${}^2F_{7/2} \rightarrow {}^2F_{5/2}$ transition of Yb^{3+}[24].

Figure 14 shows the magnetic field dependence of $\Delta E_{R'}(H_0) - \Delta E_R(H_0)$ and $\Delta E_{\mathrm{Yb}}(H_0)$. The negative deviation of $\Delta E_{R'}(H_0) - \Delta E_R(H_0)$ from $\Delta E_{\mathrm{Yb}}(H_0)$ is caused by the attractive force between the Cr^{3+} exciton and the Yb^{3+} magnon. As shown

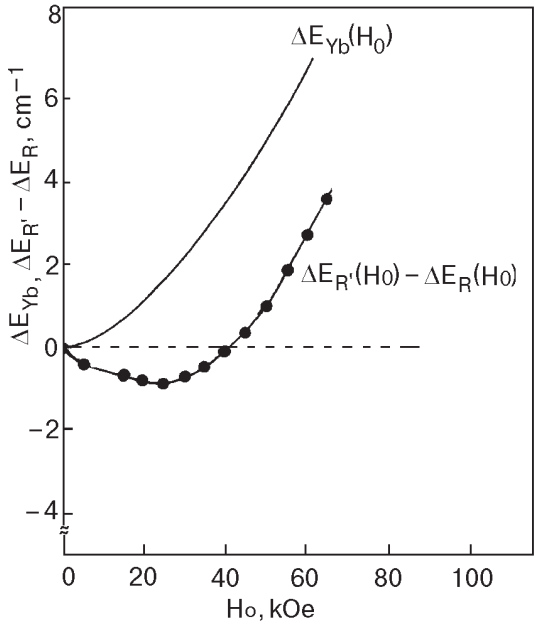

Fig. 14. Comparison between experimentally obtained values of $\Delta E_{\mathrm{Yb}}(H_0)$ and $\Delta E_{R'}(H_0) - \Delta E_R(H_0)$. The descriptions of $\Delta E_{\mathrm{Yb}}(H_0)$, $\Delta E_{R'}(H_0)$ and $\Delta E_R(H_0)$ are shown in the text.

in Fig. 14, the attractive force becomes to be strongest at 25 kOe, where the Cr^{3+} exciton–Yb^{3+} magnon at the Brillouin-zone boundary is most strongly localized. Therefore, the bound state of the R' band grows most strongly at 25 kOe.

In the case that the bound state begins to migrate, the bound state distinguishes four Cr^{3+} sites in the unit cell. Therefore, in the process of the delocalization of the bound state, the bound state exhibits the Davydov splitting. In fact, as shown in Fig. 13, the bound state of the R' band splits above 30 kOe. Therefore, we arrived at the following conclusion. In the magnetic field region above 30 kOe, the zone-edge Cr^{3+} exciton coupled with Yb^{3+} magnon begins to migrate, which reflects upon the splitting of the bound state and the significant decrease in its intensity.

At the metamagnetic transition (H_c = 67 kOe), the weak ferromagnetic moment of the Cr^{3+} spins reverses its direction, where the antisymmetric exchange interaction between the Cr^{3+} and Yb^{3+} spins, $\mathbf{D}(\mathbf{S}^{Cr} \times \mathbf{S}^{Yb})$, changes discontinuously in its sign and intensity. The change of the antisymmetric exchange interaction between the Cr^{3+} and Yb^{3+} spins at H_c should be responsible for the drastic change of the R' band. Above H_c, the shape of the R' band resembles closely the density of states of the Cr^{3+} exciton coupled with the Yb^{3+} magnon, which implies that the cooperative excitation behaves as a two-particle continuous state above H_c. Therefore, it is concluded that the Cr^{3+}–Yb^{3+} antisymmetric exchange interaction between the Cr^{3+} exciton and the Yb^{3+} magnon is attractive below H_c. On the contrary, its attractive force vanishes above H_c.

3.2. Cooperative excitation between Cr^{3+} *exciton and* Yb^{3+} *exciton*

Figure 15 shows the absorption spectra in the energy region between 23800 cm^{-1} and 24000 cm^{-1}. These spectra correspond to the cooperative transition consisting of the ${}^4A_{2g} \rightarrow {}^2E_g$ transition of Cr^{3+} and the ${}^2F_{7/2} \rightarrow {}^2F_{5/2}$ transition of Yb^{3+} in $YbCrO_3$. The average energy of the R lines is 13695.6 cm^{-1}. Since this Cr^{3+} exciton has a negative energy dispersion of −16 cm^{-1}, the energy of the Cr^{3+} exciton at the Brillouin-zone boundary is estimated at 13679.6 cm^{-1}. On the other hand, the lowest energy of the ${}^2F_{7/2} \rightarrow {}^2F_{5/2}$ transition of Yb^{3+} is 10164.6 cm^{-1}[24]. The sum of the energies of the Cr^{3+} exciton and the Yb^{3+} exciton at the Brillouin-zone boundary is estimated at 23844.2 cm^{-1}, which is almost equal to the energy of the A_1 line (23836.0 cm^{-1}) in Fig. 15. The A and B bands are assigned as shown in the inset of Fig. 15.

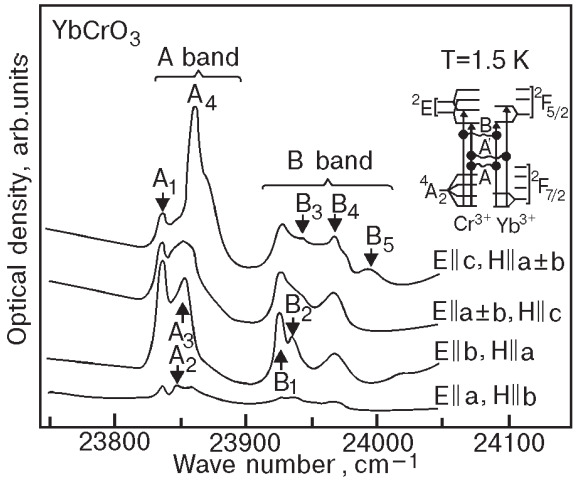

Fig. 15. Optical absorption spectra of $YbCrO_3$ at 1.5 K. E and H denote the electric and magnetic vectors of the incident light, respectively.

Figure 16 shows the behavior of the A and B bands under the magnetic field along the a axis. As shown in Fig. 16, at the metamagnetic transition H_c(= 67 kOe), the profile of the A band drastically changes. In particular, above H_c, a sharp and

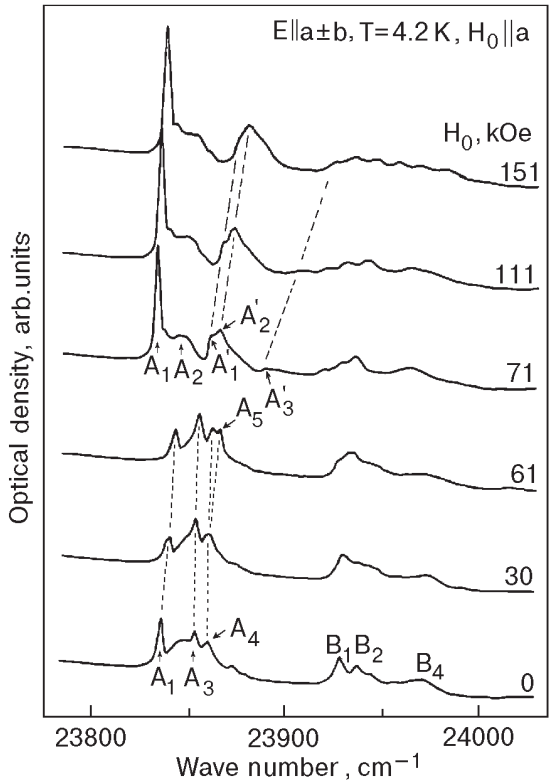

Fig. 16. Magnetic field dependence of the A and B bands of $YbCrO_3$ at 4.2 K.

strong peak typical of bound state appears on the low-frequency edge of the A band. Since the energy dispersion of the Cr^{3+} exciton corresponding to the ${}^4A_{2g} \rightarrow {}^2E_g$ transition is -16 cm^{-1}, the low-frequency edge of the A band corresponds to the Cr^{3+}–Yb^{3+} exciton molecule at the Brillouin-zone boundary. From the appearance of the bound state on the low-frequency edge of the A band above H_c, it is considered that the Cr^{3+}–Yb^{3+} exciton molecule at the Brillouin-zone boundary is strongly localized above H_c.

As mentioned already, the Cr^{3+}–Yb^{3+} antisymmetric exchange interaction, $\mathbf{D}(\mathbf{S}^{Cr} \times \mathbf{S}^{Yb})$, in $YbCrO_3$ creates various cooperative excitations between the Cr^{3+} and Yb^{3+} elementary excitations. In the case of Cr^{3+} exciton–Yb^{3+} exciton system, the Cr^{3+}–Yb^{3+} antisymmetric exchange interaction acts as a strong attractive force above H_c. Contrary to this, it acts on the Cr^{3+} exciton–Yb^{3+} magnon system as a strong attractive force below H_c. From this result, the sign of the antisymmetric exchange interaction between the Cr^{3+} exciton (${}^2E_g$) and the Yb^{3+} exciton (${}^2F_{5/2}$) is presumed to be different from that between the Cr^{3+} exciton (${}^2E_g$) and the Yb^{3+} magnon (${}^2F_{7/2}$).

4. Photo-induced magnetism

One of the recent topics of solid state physics is photo-induced transformation of electronic and magnetic state of matters. The magnetic states of several compounds such as $[Fe(ptz)_6](BF_4)_2$ (ptz = 1-propyltetrazole)[27], $K_{0.4}Co_{1.3}[Fe(CN)_6]\cdot 5H_2O$ [28],(In,Mn)As/GaSb [29], have been revealed to be transformed to another states by photo-irradiation. In the case of $[Fe(ptz)_6](BF_4)_2$, the ground state of Fe(II) is converted between the low-spin state ($t_2{}^6$, $S = 0$) and the high spin state ($t_2{}^4e^2$, $S = 2$) by the photo-irradiation corresponding to the d–d transition [27,30]. In the case of $K_{0.4}Co_{1.3}[Fe(CN)_6]\cdot 5H_2O$ [28], this compound can be switched reversibly back and forth between ferrimagnetism and paramagnetism by the photo-irradiation corresponding to the charge transfer transition between the Co and Fe sites. In a novel III–V-based magnetic semiconductor heterostructure p-(In,Mn)As/GaSb grown by molecular beam epitaxy, the ferromagnetic order is induced by photo-generated carriers [29].

These studies on photo-induced magnetism are creating a new field of solid state physics. In connection with photo-induced magnetism, pioneering works have been done by Tsushima et al. [31,32]. Kovalenko et al. [33,34] and Golovenchitz et al. [35]. For instance, Kovalenko et al. have found that the linearly polarized illumination of yttrium iron garnet, $Y_3Fe_{5-x}Si_xO_{12}$, results in a spin-reorientation transition as a result of the photo-induced change of the crystalline magnetic anisotropy [33,34]. On the other hand, Tsushima et al. have observed a photo-induced spin-reorientation transition from the antiferromagnetic to the weak-ferromagnetic spin structure of $ErCrO_3$ by using a time-resolved spectroscopic method [31,32]. In this Section, we describe the photo-induced spin-reorientation from $\Gamma_1(A_xG_yC_z;C_z^R)$ to $\Gamma_4(G_xA_yF_z;F_z^R)$ for $ErCrO_3$.

Now, we briefly summarize the magnetic properties of $ErCrO_3$. $ErCrO_3$ is magnetically ordered below T_{N1} = 133 K with a weak-ferromagnetic structure denoted as $\Gamma_4(G_xA_yF_z;F_z^R)$ [36]. At 9.8 K, $ErCrO_3$ exhibits the temperature induced spin-reorientation from $\Gamma_4(G_xA_yF_z;F_z^R)$ to $\Gamma_1(A_xG_yC_z;C_z^R)$, where the ferromagnetic moment disappears. Below 9.8 K, the Γ_4 phase can be recovered by applying a small external magnetic field ($H_0 < 1.5$ kOe) along the c axis [37,38].

In order to generate the photo-induced spin-reorientation, we used a Q-switched ruby laser (6943 Å, 25 ns in half width and output power of a few mJ) as a photo-irradiation source. The absorption spectrum of Er^{3+} in $ErCrO_3$ was observed at 1.8 K to detect the photo-induced spin-reorientation transition from $\Gamma_1(A_xG_yC_z;C_z^R)$ to $\Gamma_4(G_xA_yF_z;F_z^R)$. Figure 17,*a* shows the energy levels and the selection rule for the electric dipole transitions between the ${}^4I_{15/2}$ (denoted I' and I'') ground state and the ${}^4I_{9/2}$ (denoted b' and b'') excited state of Er^{3+} in $ErCrO_3$. As shown in the figure, the absorption spectrum for this transition is composed of four lines, which we label $I'b'$, $I'b''$, $I''b'$ and $I''b''$. In the $\Gamma_1(A_xG_yC_z;C_z^R)$ spin configuration, the $I'b'$ and $I''b''$ absorption lines are superimposed because $\Delta E(I) \sim \Delta E(b) \sim 10$ K. The four lines, however, are well resolved in the $\Gamma_4(G_xA_yF_z;F_z^R)$ spin configuration. For the case of $E \perp c$, the absorption lines, $I'b'$ and $I''b''$, are observed at 8049 Å associated with the $\Gamma_1(A_xG_yC_z;C_z^R)$ spin configuration. In the $\Gamma_4(G_xA_yF_z;F_z^R)$ spin configuration, these absorption lines are observed at 8045 and 8054 Å. Figure 17,*b* shows the time-resolved Ib absorption spectra after initial laser excitation at 7 K. It can be seen that $ErCrO_3$ undergoes a phase transition from $\Gamma_1(A_xG_yC_z;C_z^R)$ to $\Gamma_4(G_xA_yF_z;F_z^R)$ within 50 μs after the photo-irradiation, and that it returns to the $\Gamma_1(A_xG_yC_z;C_z^R)$ phase in about 400 ms after the irradiation.

The idea of photo-induced spin-reorientation transition has been raised from the following argument. In many $RCrO_3$ and $RFeO_3$, the direction of the easy axis of magnetization easily changes as the temperature changes or an external magnetic field

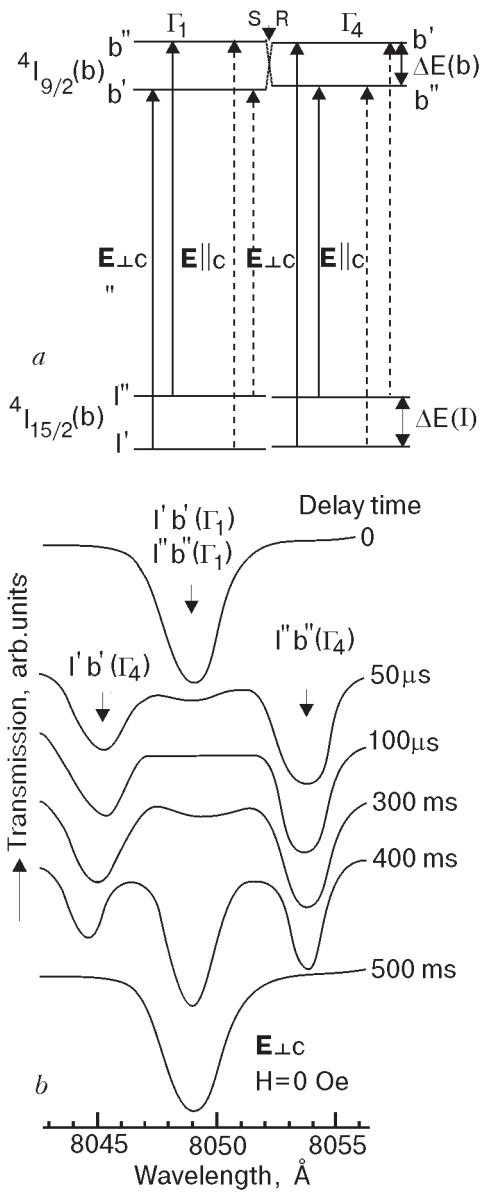

Fig. 17. (*a*) Schematic energy level diagram for the ${}^4I_{15/2}(I) \rightarrow {}^4I_{9/2}(b)$ transitions of $ErCrO_3$. Also shown are optical transitions and their polarization. (*b*) Time-resolved *Ib* absorption spectra after initial laser excitation.

is applied. It is expected that the critical temperature of spin-reorientation is changed when some of the magnetic ions are substituted by magnetic impurities. For example, $YFe_{1-x}Co_{x/2}Ti_{x/2}O_3$ (x= 0.003) undergoes the spin-reorientation from $\Gamma_2(F_xC_yG_z)$ to Γ_4 ($G_xA_yF_z$) at 247 K, while $YFeO_3$ does not show any spin-reorientation [39]. The magnetic anisotropy of $YFeO_3$ influenced by small amount of Co^{2+} is responsible for the appearance of spin-reorientation in-$YFe_{1-x}Co_{x/2}Ti_{x/2}O_3$($x$=0.003) [40]. Therefore, the photo-irradiation is regarded as a transient substitution of the magnetic ions by magnetic impurities, which presumably induces the phase transition when the sample is kept near the critical temperature. However, in general, both of thermo-magnetic effect and transient impurity effect are induced by laser irradiation. The transient impurity effect is justified if the phase transition is induced before any non-radiative and radiative decay of the photo-excited state occurs. Since the life time of the ${}^2E_g$ state of Cr^{3+} is quite long (several ms), the photo-irradiation corresponding to the ${}^4A_{2g} \rightarrow {}^2E_g$ transition of Cr^{3+} in $ErCrO_3$ is the most effective to generate the photo-induced spin-reorientation transition. In order to further prove the transient impurity effect, the time-resolved spectroscopic measurement by using ultrashort laser (femtosecond laser) will be indispensable.

Finally, in connection with photo-induced magnetism, it should be noted that in some crystals of the family of antiferromagnetic garnets $Ca_3Mn_2Ge_3O_{12}$ etc., photo-induced phenomena have been discovered by Eremenko, Gnatchenko et al. [41– 44]. Photo-irradiation with visible light results in arising of long-lived changes: linear birefringence, magnetic moment in the antiferromagnetic state, augmentation of optical absorption coefficient. The revealed photo-induced changes of optical and magnetic properties in antiferromagnetic garnets persist for a long time after switching off illumination. The discovery of sufficiently great photo-induced changes of refractive index and absorption coefficient in antiferromagnetic garnets will create a new field of optical and magneto-optical recording.

5. Recent frontier research on application

We shall describe briefly about a recent research on application of magneto-optical materials using their unique magneto-optical non-reciprocity. The most advantageous uniqueness of magneto-optical materials lies in a fact that a propagation of the light in those magnetic materials is antisymmetric (non-reciprocal) to an inversion of time.

One is on highly bismuth-substituted rare-earth iron garnets in a near-infrared wave-length region for optical isolators and circulators [45,46]. The other is on a diluted magnetic semiconductors, such as CdMnTe in a more shorter wave-length region for integrated magneto-optical waveguides [47]. A schematic figure of an achieved integrated magneto-optical guide on GaAs substrate by Zaets and Ando is shown in Fig. 18 [48].

Finally, in addition to the above, a so-called magneto-optical recording has become a real device for a rewritable high density non-volatile memory. It shows more development year by year. The most recent progress in the magneto-optical recording for

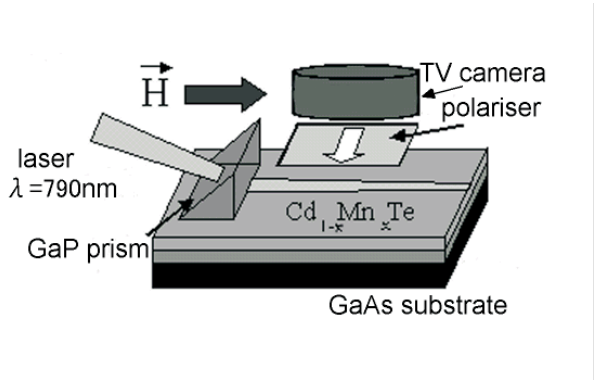

Fig.18. Magneto-optical waveguide of $Cd_{1-x}Mn_xTe$ on GaAs substrate. TE mode scattered light from a surface of waveguide is observed by illuminating TM mode laser with λ= 790 nm (Ref. 48).

more high density recording, including super-resolution limit recording density smaller than a domain size has been reviewed in a recent book by Kaneko [49].

6. Conclusion

We have investigated various kinds of magneto-optical properties for rare earth orthochromites. In $RCrO_3$(R = Tb, Dy and Ho), from the analysis of Cr^{3+} exciton absorption, we have elucidated that these compounds exhibit an anomalous spin-reorientation under the magnetic field along the *b* axis, where the weak ferromagnetic moment of the Cr^{3+} spins rotates in the *ac* plane perpendicular to the *b* axis. It is quite difficult to elucidate the microscopic mechanism of this phase transition by means of magnetization measurement.

In $RCrO_3$(R= Dy and Ho), we have elucidated the breakdown of the **k** = 0 selection rule for the Cr^{3+} exciton absorption induced by the disorder of the R^{3+} spin configuration. The magneto-elastic effect due to the R^{3+}(R = Dy and Ho) ion is extraordinarily large because of the strong spin-orbit interaction. Through the medium of this strong magneto-elastic effect, the disorder of the R^{3+} spin configuration causes the breakdown of the **k**=0 selection rule of the Cr^{3+} exciton absorption, which is reflected in the appearance of the anomalous satellite band (*R′*) in the lower energy side of the free Cr^{3+} exciton absorption.

In $YbCrO_3$, we have observed various kinds of cooperative excitations such as Cr^{3+} exciton coupled with Yb^{3+} magnon, and Cr^{3+}–Yb^{3+} exciton molecule in the visible region, which are induced by the antisymmetric exchange interaction between the Cr^{3+} and Yb^{3+} spins. In these cooperative excitations, the Cr^{3+}–Yb^{3+} antisymmetric exchange interaction acts as a strong attractive force, which is responsible for the appearance of the bound state in the lower frequency edge in the cooperative excitations.

In $ErCrO_3$, a photo-induced spin-reorientation from Γ_1 to Γ_4 takes place within 50 μs after the photo-irradiation corresponding to the ${}^4A_{2g} \rightarrow {}^2E_g$ transition of Cr^{3+}, and it returns to the initial spin configuration in about 400 ms. This phenomenon was detected by the time-resolved Er^{3+} absorption spectra corresponding to the ${}^4I_{15/2} \rightarrow {}^4I_{9/2}$ transition. The photo-irradiation is regarded as a transient substitution of the magnetic ions by magnetic impurities, which presumably induces the phase transition. In order to further prove the transient impurity effect, the time-resolved spectroscopic measurement by using ultrashort laser will be indispensable.

Finally, in connection with the recent topics of magneto-optics such as optical isolator, integrated magneto-optical waveguide and magneto-optical recording, we briefly reviewed the recent frontier research on application mainly developed in Japan.

Acknowledgments

The authors would like to thank many scientists who have given us an opportunity and collaborated with us for a long time of our recent work. Some of them are S. Sugano, I. Tsujikawa, K. Aoyagi, H. Kamimura, W. M. Yen, T. Tamaki, N. Watanabe, J. Dillon Jr., K. V. Rao, P. L. Richards, M. Pardavi-Horvath, and H. Szymczak

V. V. Eremenko is undoubtedly to be specially cited as an exclusively intimate physicist among those. The authors also would like to express to thank many other younger research colleagues for a pleasant collaboration in many subjects in many occasions.

This work was partly supported by the Science and Technical Research Laboratories of Japan broadcasting Corporation, and a Grant-in Aid for Science Research from the Ministry of Education, Science, Sports and Culture.

1. *Adv. in Magneto-Optics, Proc. Int. Symp. Magneto-Optics*, *J. Mag. Soc. Jpn.*, **11**, Supplement, S1, (1987).
2. *Adv. in Magneto-Optics, Proc. 2nd Int. Symp. Magneto-Optics, Fiz. Nizk. Temp.* **18**, Supplement, No. S1, (1992).
3. V. V. Eremenko, N. F. Kharchenko, Yu. G. Litvinenko, and V. M. Naumenko, *Magneto-Optics and Spectroscopy of Antiferromagnets*, Springer-Verlag (1992).
4. A. K. Zvezdin and V. A. Kotov, *Modern Magnetooptics and Magnetooptical Materials,* Institute of Physics Publishing (1997).

5. S. Sugano and N. Kojima (ed.), *Magneto-Optics*, Springer (2000).
6. S. Quezel-Ambrunaz and M. Mareschal, *Bull. Soc. Fr. Mineral. Cristallogr*. **LXXXVI**, 204 (1963).
7. E. F. Bertaut, in: *Magnetism III*, G. T. Rado and H. Suhl (eds.), Academic, New York (1963), p. 149.
8. R. Courths and S. Hüfner, *Z. Phys*. **B24**, 193 (1976).
9. N. Kojima, I. Tsujikawa, and K. Tsushima, *Proc. Int. Conf. Ferrites*, Kyoto (1980), p. 769.
10. R. M. Hornreich, B. M. Wanklyn, and I. Yaeger, *Int. J. Magn*. **2**, 77 (1972).
11. E. F. Bertaut, J. Mareschal, and G. F. de Vries, *J. Phys. Chem. Solids* **28**, 2143 (1967).
12. J. D. Gordon, R. M. Hornreich, S. Shtrikman, and B. M. Wanklyn, *Phys. Rev*. **B13**, 3012 (1976).
13. K. Tsushima, T. Tamaki, and R. Yamaura, *Proc. Int. Conf. Magnetism*: *ICM-73*, Nauka, Moscow (1974) **5**, p. 270.
14. Y. Uesaka, I. Tsujikawa, K. Aoyagi, K. Tsushima, and S. Sugano, *J. Phys. Soc. Jpn*. **31**, 1380 (1971).
15. B. L. Joesten and F. C. Brown, *Phys. Rev.* **148**, 919 (1966).
16. S. Lai and M. V. Klein, *Phys. Rev. Lett.* **44**, 1087 (1980).
17. M. V. Klein, M. D. Sturge, and E. Cohen, *Phys. Rev*. **B25**, 4331 (1982).
18. N. Kojima, I. Tsujikawa, K. Aoyagi, and K. Tsushima, *J. Phys. Soc. Jpn.* **54**, 4804 (1985).
19. N. Kojima, I. Tsujikawa, and K. Tsushima, *J. Phys. Soc. Jpn*. **54,** 4794 (1985).
20. N. Kojima, K. Aoyagi, K. Tsushima, I. Tsujikawa, and S. Sugano, *J. Phys. Soc. Jpn*. **49,** 1463 (1980).
21. R. L. Greene, D. D. Sell, W. M. Yen, A. L. Schawlow, and R. M. White, *Phys. Rev. Lett*. **15**, 656 (1965).
22. N. Kojima, H. Okada, M. Kawarazaki, I. Mogi, M.Takeda, G. Kido, Y. Nakagawa, and K. Tsushima, *J. Phys. Soc. Jpn.* **64**, 3082 (1995).
23. N. Kojima, M. Kawarazaki, H. Okada, I. Mogi, M. Takeda, G. Kido, Y. Nakagawa, and K. Tsushima, *J. Phys. Soc. Jpn.* **64**, 3090 (1995).
24. N. Kojima, K. Tsushima, and I. Tsujikawa, *J. Phys. Soc. Jpn*. **49**, 1449 (1980).
25. S. Shtrikman, B. M. Wanklyn, and I. Yaeger, *Int. J. Mag.* **1**, 327 (1971).
26. N. Kojima, K. Tsushima, S. Kurita, and I. Tsujikawa, *J. Phys. Soc. Jpn.* **49**, 1456 (1980).
27. S. Decurtins, P. Gütlich, C. P. Köhler, H. Spiering, and A. Hauser, *Chem. Phys. Lett.* **105**, 1 (1984).
28. O. Sato, T. Iyoda, A. Fujishima, and K. Hashimoto, *Science* **272**, 704 (1996).
29. S. Koshihara, A. Oiwa, M. Hirasawa, S. Katsumoto, Y. Iye, C. Urano, H. Takagi, and H. Munekata, *Phys. Rev. Lett.* **78**, 4617 (1997).
30. A. Hauser, *Chem. Phys. Lett,* **124**, *545 (1986).*
31. S. Kurita, K. Toyokawa, K. Tsushima, and S. Sugano, *Solid State Commun*. **38**, 235 (1981).
32. T. Tamaki and K. Tsushima, *J. Magn. Magn. Mater.* **31–34**, 571 (1983).
33. V. F. Kovalenko, E. S. Kolezhuk, and P. S. Kuts, *Sov. Phys. JETP* **54**, 742 (1981).
34. V. F. Kovalenko, P. S. Kuts, and V. P. Sokhatskii, *Sov. Phys. Solid State* **24,** 80 (1982).
35. E. I. Golovenchitz and V. A. Sanina, *Fiz. Tverd. Tela,* **24**, 375 (1982).
36. M. Eibschütz, L. Holmes, J. P. Maita, and L. G. Van Uitert, *Solid State Commun.* **8**, 1815 (1970).
37. M. Kaneko, S. Kurita, and K. Tsushima, *J. Phys. Solid State Phys.* **10,** 1979 (1977).
38. K. Toyokawa, S. Kurita, and K. Tsushima, *Phys. Rev.* **B19,** 274 (1979).
39. H. Makino and Y. Hidaka, *IEEE Trans. Magnetics,* **MAG-8**, 444 (1972).
40. M. Abe, K. Kaneta, M. Gomi, Y. Mori, and S. Nomura, *Jpn. J. Appl. Phys.* **16**, 1799 (1977).
41. V. V. Eremenko, S. L. Gnatchenko, I. S. Kachur, V. G. Piryatinskaya, A. M. Ratner, and V. V. Shapiro, *Phys. Rev.* **B61**, 10670 (2000).
42. V. V. Eremenko, S. L. Gnatchenko, I. S. Kachur, V. G. Piryatinskaya, M. B. Kosmyna, B. P. Nazarenko, and V. M. Puzikov, *Appl. Phys. Lett*. **79**, 734 (2001).
43. V. V. Eremenko, S. L. Gnatchenko, I. S. Kachur, V. G. Piryatinskaya, A. M. Ratner, V. V. Shapiro, M. Fally, and R. A. Rupp, *Fiz. Nizk. Temp.* **27**, 30 (2001) [*Low Temp. Phys.* **27**, 22 (2001)].
44. V. A. Bedarev, V. I. Gapon, S. L. Gnatchenko, M. Baran, R. Szymczak, J. M. Desvignes, and H. Le Gall, *Fiz. Nizk. Temp.,* **28**, 51 (2002) [*Low Temp. Phys*. **28**, 37 (2002)].
45. K. Tsushima: *Growth of a Highly Bismuth-Substituted Rare-earth Iron Garnet and its Application to an Optical Isolator,* in: *Japan Annual Reviews in Electronics, Computers Tele-Communications,* **21.**, *Recent Magnetics for Electronics*, Y. Sakurai (ed), Ohmsha & North-Holland Amsterdam & Tokyo (1985/1986), p. 113
46. A general review is given, for example, by K. Shinagawa: *Faraday and Kerr Effects in Ferromagnets, Magneto-Optics, Springer Series in Solid State Sciences,* **128**, S. Sugano and N. Kojima (eds.) (2000), p. 137
47. A general review is given, for example, by K. Ando*: Magneto-Optics of Diluted Magnetic Semiconductors: New Materials and Applications, Magneto-Optics*, *Springer Series in Solid State Sciences*, **128**, S. Sugano and N. Kojima (eds.) (2000), p. 211
48. W. Zaets and K. Ando, Appl. *Phys. Lett.* **77**, 1593 (2000).
49. A general review is given, for example, by M. Kaneko: *Magneto-Optical Recording, Magneto-Optics, Springer Series in Solid State Sciences*, **128**, S. Sugano and N. Kojima (eds) (2000), p. 271